Model for the electronic and vibronic structure of $^4T_1$ levels of d^5 ions coupled to E vibrational modes: Case of the fluorescent level of Mn^{2+} in ZnS

R. Parrot
Université des Antilles Guyane, Institut Universitaire de Formation des Maîtres et Faculté de Technologie de la Guyane, Boite Postale 792, 97337 Cayenne Cedex, Guyane, France

D. Boulanger
Université de Paris–Sud, Laboratoire d'Informatique, Maîtrise de Sciences Physiques, Bâtiment 479, 91405 Orsay Cedex, France

M. N. Diarra
Université de Dakar, Département de Physique, Dakar-Fann, Senegal

U. W. Pohl, B. Litzenburger, and H. E. Gumlich
Technical University of Berlin, Institute of Solid State Physics, Hardenbergstrasse 36, D-1000 Berlin 12, Germany
(Received 10 August 1995; revised manuscript received 23 January 1996)

The four fundamental vibronic lines of a $^4T_1$ level of a d^5 ion coupled to E vibrational modes in cubic symmetry have been observed. An analysis of the four fine-structure lines of the fluorescent level $^4T_1$ of Mn^{2+} in cubic ZnS, which have been observed at high resolution in pure cubic ZnS crystals, shows that the relative energies and dipole strengths (RDS) of the quasidegenerate levels are not those predicted by previous electronic and vibronic models. A model is elaborated in three steps. First, from Ham's model for the coupling of orbital triplet states to E modes, a phenomenological operator describing the first-order and second-order spin-orbit interaction and the spin-spin interaction in terms of three parameters is proposed to account for the energy levels and the RDS's. Two phenomenological descriptions deduced from an analysis of the RDS are proposed for the studied state. Second, a detailed analysis of the spin-orbit and spin-spin interactions in terms of the Huang-Rhys factor and of the energy of the effective phonons shows that the electronic spin-orbit interaction in $\boldsymbol{l}\cdot\boldsymbol{S}$ is of opposite sign to that predicted by the model restricted to the d^5 configuration. Finally, a covalent model involving the molecular spin-orbit interaction defined by Misetich and Buch is developed to account for the first-order spin-orbit splitting of the orbital triplet states of Mn^{2+} in II-VI compounds. [S0163-1829(96)03927-6]

I. INTRODUCTION

The influence of the dynamical Jahn-Teller (JT) effect on the fine-structure lines of the orbital doublet and triplet states of d^n ions in crystals and molecules has long been studied either theoretically or experimentally.[1–4] Very sophisticated molecular orbital theories as well as simplified semiemperical models have also been developed to analyze the fundamental and excited levels of d^n ions.[5,6]

Concerning Mn^{2+} ions, the fine structure of the fluorescent level $^4T_1(G)$ at lower energy and, in some cases, of the multiplets $^4T_2(G)$, $^4E(G)$ at higher energy has been studied in II-IV (Refs. 7–9) and III-V (Ref. 10) compounds as well as in organic,[11] magnetic,[12] and other compounds.[13]

In the case of Mn^{2+} in II-VI compounds, it has long been shown that the electronic and vibronic structures of the orbital triplets $^4T_1(G)$, $^4T_2(G)$, and orbital doublet $^4E(G)$ were much more puzzling than expected.

In a theoretical study on the $^4T_1(G)$ and $^4T_2(G)$ levels of Mn^{2+} in II-VI and III-V compounds, published two decades ago, Koidl[14] proposed to interpret the experimental structure of the fluorescent levels $^4T_1(G)$ of Mn^{2+} in ZnS [two lines separated by 9.6 cm^{-1} (Ref. 7)], ZnSe [two lines separated by 10 cm^{-1} (Ref. 8) instead of 20 cm^{-1} (Ref. 9)], CdS [axial symmetry, two lines separated by 10 cm^{-1} (Ref. 9)], and GaP [two lines separated by 12 cm^{-1} (Ref. 10)], and of the $^4T_2(G)$ level in ZnS [two lines separated by 3 cm^{-1} (Ref. 7)], and ZnSe [two lines separated by 10 cm^{-1} (Ref. 9)], in terms of a strong coupling to E modes. The argument, based on Ham's model for the coupling of orbital triplet states to E modes,[1] was that near the strong coupling limit, the fundamental vibronic structure of a $^4T_1$ level consists of two groups of two lines, one group being associated to the quasidegenerate states $|\Gamma_6\rangle$ and $|\Gamma_8'(5/2)\rangle = (1/\sqrt{10})|\Gamma_8(3/2)\rangle + (3/\sqrt{10})|\Gamma_8(5/2)\rangle$ and the other to the quasidegenerate states $|\Gamma_7\rangle$ and $|\Gamma_8'(3/2)\rangle = (3/\sqrt{10})|\Gamma_8(3/2)\rangle - (1/\sqrt{10})|\Gamma_8(5/2)\rangle$ (see Fig. 1). In the case of a $^4T_2$ level, the quasidegenerate states are $|\Gamma_7\rangle$, $|\Gamma_8'(5/2)\rangle$ and $|\Gamma_6\rangle$, $|\Gamma_8'(3/2)\rangle$. The energy separation between the two groups of lines is due to the nonreduced second-order spin-orbit interaction between the fundamental vibronic states $|^4T_1\rangle$ or $|^4T_2\rangle$ and the other electronic states of the ion. The experimental evidence of a coupling to E modes was not yet established but the hypothesis of a strong coupling to E modes was the simplest to account for an almost complete quenching of the first-order spin-orbit interaction and of the coupling to T_2 strains. Moreover, the energy separation between the observed lines, as predicted by the crystal-field (CF) model, was in good agreement with experi-

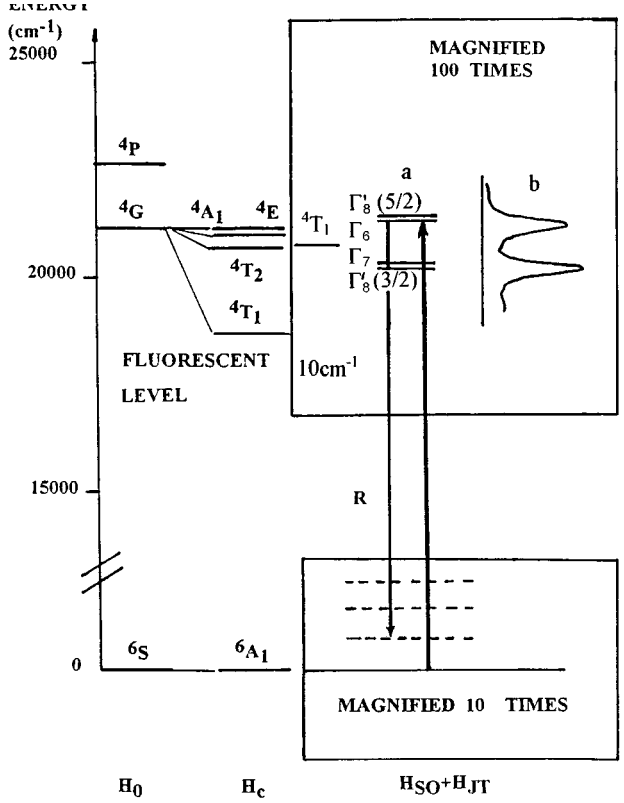

FIG. 1. The lowest energy levels of Mn^{2+} in cubic ZnS, as given by the free ion Hamiltonian H_0 and the cubic crystal field H_c, are given to the left. The upper inset (a) gives the influence of the spin-orbit interaction and of the Jahn-Teller coupling to E modes as predicted by the previous model for the structure of the fluorescent $^4T_1$ level. The excitation spectrum of the $^4T_1$ level as given by previous experiments (Refs. 8 and 17) is represented in (b). The very small spin-orbit splitting of the fundamental state is not represented. R represents radiative transitions from the $^4T_1$ level to phonon assisted lines of the fundamental $^6A_1$ level. To simplify the reading of the figure, the shift of the $^4T_1$ level due to the Jahn-Teller energy is not represented.

ments. Therefore, this simple and unified interpretation for the vibronic structure of the orbital triplet states of Mn^{2+} in II-VI and III-V compounds seemed plausible and it did not seem necessary to question the CF model, which accounted very well for the splitting of the observed lines.

Unfortunately, uniaxial stress experiments performed concomitantly by Parrot, Naud, and Gendron[15] on the $^4T_2(G)$ level of Mn^{2+} in ZnS and ZnSe very surprisingly showed that the structure of this state was not at all that corresponding to a strong JT coupling to E modes as expected. Experiments clearly demonstrated that this state was effectively coupled to E modes but that the two lines of the $^4T_2(G)$ level of Mn^{2+} behaved under uniaxial stresses as two electronic levels Γ_8 and Γ_6. A very detailed study leading to the diagonalization of vibronic matrices involving up to 5 phonons of symmetry E_θ and E_ϵ led these authors to consider a intermediate coupling to E modes, corresponding to a Huang-Rhys factor of 0.6, and a selective intensity transfer for the level Γ_8 at higher energy, the transition $^6A_1 \rightarrow \Gamma_7$ being forbidden by symmetry. Furthermore, it was shown that in the case of Mn^{2+} in ZnSe selective intensity transfer can be accounted for only by considering a first-order spin-orbit splitting 2.4 times greater than that predicted by the model restricted to the d^5 configuration. These experiments clearly showed that Koidl's basic assumption of a *strong* coupling to E modes was not verified. This means that due to the lack of theoretical models able to predict with certainty the strength of the coupling to E and/or T_2 modes, experiments only can give the nature of the coupling. Another very important result of this study was that only a ligand-field (LF) model involving the molecular spin-orbit interaction could give a unified interpretation for the first-order spin-orbit coupling of Mn^{2+} in ZnS, ZnSe, and other compounds.

The electronic structure of the $^4E(G)$ level of Mn^{2+} was revealed to be even more puzzling than the structure of the $^4T_2(G)$ level. Uniaxial stress experiments on the $^4E(G)$ level of Mn^{2+} in ZnS, ZnSe, and studies of the influence of internal strains in nearly tetrahedral clusters such as $MnCl_4$ and MnB_4 showed unambiguously that the CF model had to be rejected.[16] All experimental results were interpreted in terms of a linear coupling to E modes or to internal strains of E symmetry, while the CF model predicts that first-order linear couplings to E strains and T_2 strains are forbidden by seniority and symmetry, respectively, and that second-order perturbation schemes predict a linear coupling to T_2 strains and a quadratic coupling to E strains.

Further experimental studies on the uniaxial stress effect on the two experimental lines associated to the fluorescent level $^4T_1(G)$ of Mn^{2+} in ZnS and ZnSe (Ref. 8) were interpreted in terms of a strong coupling to E modes. Experiments on the magnetic field effect on this level of Mn^{2+} in ZnS (Ref. 17) and GaP (Ref. 18) were performed and interpreted in terms of the Zeeman Hamiltonian $\mu_B \mathbf{H} g \mathbf{S}$. In these studies the structure of the quasidegenerate states was not observed.

It will be shown here that the structure of the fluorescent $^4T_1(G)$ level of Mn^{2+} in ZnS and other II-VI compounds is different from that considered previously, and that covalency plays a dominant role in the structure of this level as it does for the structure of the levels $^4T_2(G)$ and $^4E(G)$.

The complexity of the structure of the orbital triplet $^4T_2(G)$ of Mn^{2+} and the fact that the complete fine structure of the $^4T_1(G)$ level of Mn^{2+} in ZnS is not that expected from the previous model, led us to adopt a very critical position with respect to the explicit and implicit assumptions of this model. In the following analysis we will carefully avoid assumptions not confirmed by experimental results, analyze all possible indexations of experimental lines that can account for the experimental spectrum, and reject analogies as well as generalizations that can be very misleading.

The samples, the apparatus, and the experimental results are described in Sec. II.

The experimental results are compared to the previous model for the dynamical JT effect on $^4T_1$ levels in Sec. III. A detailed analysis, in terms of the Huang-Rhys factor, of the JT reduction of the first- and second-order spin-orbit interactions restricted to the d^5 configuration is performed first. Then, by analyzing the relative dipole strengths (RDS), it is shown that the energies of the quasidegenerate states cannot be accounted for from this model.

Section IV is devoted to a critical analysis of the electronic and vibronic structure of orbital triplets of d^5 ions.

First, semiquantitative arguments suggest that the experimental spectrum could be correctly interpreted by assuming that the electronic first-order spin-orbit splitting of Mn^{2+} ions should be very strongly reduced or even of opposite sign with respect to that predicted by the CF model restricted to the d^5 configuration. Then, from symmetry considerations an equivalent operator is defined that gives the first- and second-order spin-orbit interaction and the spin-spin interaction in terms of three parameters. Finally, two phenomenological descriptions are proposed for the studied $^4T_1$ level that exactly account for the energy levels and correctly account for the RDS's.

A physical model that accounts for the electronic and vibronic interactions is presented in Sec. V. Whereas, until now, the strength of the coupling to E modes was determined from an analysis, in terms of the Huang-Rhys factor S, of the spin-orbit splitting predicted by the CF model, we proceeded in the reverse order by determining, for various values for S and for the energy of the effective phonons, which electronic spin-orbit interaction accounts for the observed vibronic structure. It is shown that, for the two proposed indexations, the spin-orbit interaction in $\boldsymbol{l}\cdot\boldsymbol{S}$ of the $^4T_1$ state of Mn^{2+} in ZnS, must be strongly reduced and inversed with respect to the splitting predicted by the CF model.

Finally, in Sec. VI, the electronic structure of the fluorescent level of Mn^{2+} in ZnS is analyzed with a very elaborate linear combination of atomic orbitals–molecular orbitals (LCAO-MO) model. This model is extended to Mn^{2+} in ZnSe to determine the trends of covalency effects in II-VI compounds. By using the molecular spin-orbit interaction defined by Misetich and Buch,[19] and the monoelectronic and multielectronic wave functions, which correctly accounted for the orbit-lattice coupling coefficients (OLCC) of this state[20] and for the spin-lattice coupling coefficients (SLCC) of the fundamental state,[21] it is shown that the first-order spin-orbit splitting of the $^4T_1(G)$ level is very strongly reduced in ZnS; it is enhanced and inversed in ZnSe with respect to that given by the previous CF model restricted to the d^5 configuration.

II. EXPERIMENT

A. Samples and apparatus

The experiments were performed on ZnS:Mn crystals grown at the Institute of Solid State Physics of the Technical University of Berlin. Great care was given to the selection of the crystals; crystals showing stacking faults,[22] Mn-Mn pair spectra,[23] or large internal strains were rejected.

For the selected crystals, no fine-structure line due to Mn^{2+} centers in stacking faults has been observed in the excitation spectra from the fundamental level to the excited levels $^4T_1$, $^4T_2$, and ^4E, thus demonstrating that the crystals are pure cubic. Furthermore, the concentration in Mn^{2+} ions was chosen to be as low as 10^{-4} mole fraction so that no fine-structure line due to Mn-Mn pairs was observed near the levels $^4T_1$ or the levels $^4T_2$ and ^4E. The fine-structure lines of the fluorescent level is the sharpest observed until now.

The excitation spectra were obtained by using polarized excitation spectroscopy. The laser system (Lambda Physik) consisted of a XeCl* excimer laser pumping a dye laser. The linewidth of the laser system was approximately 0.4 cm^{-1}.

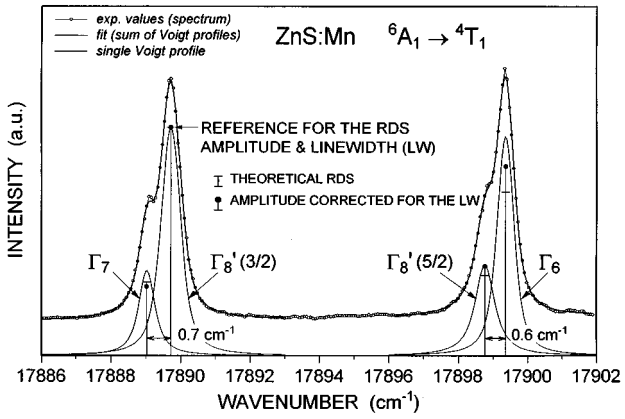

FIG. 2. Excitation spectrum of the transition $^6A_1 \rightarrow {}^4T_1(G)$ of Mn^{2+} ions in pure cubic ZnS showing the four vibronic lines of the $^4T_1(G)$ level. The indexation of the lines results from the analysis of the relative dipole strengths given in Sec. III. Another indexation obtained by permuting the indexation of the two less intense lines and of the two most intense lines is studied in Secs. IV and V.

The emission light was selected by a monochromator centered at 17 240 cm^{-1} corresponding to the maximum of the emission band.

B. Experimental spectra

The experimental spectrum given in Fig. 2 clearly shows the splittings of the quasidegenerate levels denoted Γ_6 and $\Gamma_8'(5/2)$ on one hand and Γ_7 and $\Gamma_8'(5/2)$ on the other hand. The indexation of the lines given in Fig. 2 will be called ''first indexation''; another indexation called ''second indexation'' will be considered below.

The energies and relative dipole strengths for the four levels have been obtained by carefully decomposing the superposed lines into two components. Several fitting procedures were performed using Gauss, Lorentz, and Voigt profiles. Gauss profiles did not fit the spectrum, Lorentz profiles correctly fit the top of the lines only, the best fit represented on Fig. 2 has been obtained with Voigt profiles. The errors, as given from an analysis of eight fits are ± 0.04 cm^{-1} for the energies (W), 5% for the relative amplitudes (A), and $+0.1$ cm^{-1} for the linewidths. The RDS have been calculated by taking the line $\Gamma_8'(3/2)$, which is theoretically the most intense, as the reference for the amplitudes and the linewidths. For convenience, the RDS of the reference line (calculated in the next section) is chosen to be the theoretical value of 62.5. The other theoretical RDS's are 45 for Γ_6, 20 for Γ_7, and 22.5 for $\Gamma_8'(5/2)$,

From the best fit, we get the following for the reference line $\Gamma_8'(3/2)$: $W=17\,889.72$ cm^{-1}, $A=52.6$, $RDS_{th}=62.5$, $LW=0.68$ cm^{-1}; for Γ_7: $W=17\,889.03$ cm^{-1}, $A=19.3$, $RDS_{expt}=18.6$, $RDS_{th}=20$, $LW=0.55$ cm^{-1}; for Γ_6: $W=17\,899.36$ cm^{-1}, $A=50.5$, $RDS_{expt}=52.1$, $RDS_{th}=45$, $LW=0.59$ cm^{-1}; and for $\Gamma_8'(5/2)$: $W=17\,898.77$ cm^{-1}, $A=20.7$, $RDS_{expt}=24.6$, $RDS_{th}=22.5$, $LW=0.68$ cm^{-1}.

The splittings of the quasidegenerate levels are of 0.60 cm^{-1} for the levels Γ_6 and $\Gamma_8'(5/2)$ and of 0.70 cm^{-1} for the levels Γ_7 and $\Gamma_8'(3/2)$.

It must be noted first that the same structure has been obtained for $T=4.2$ K (Fig. 2) and $T=2.0$ K and for concen-

trations in Mn^{2+} of 10^{-4} mole fraction (Fig. 2) and 3×10^{-4} mole fraction. Second, no artifact can explain the observed structures since optical experiments performed on the same crystals, in particular on the ^4E state, have led to the observation of very sharp lines, the linewidths being, in that case, limited by the resolution of 0.4 cm^{-1} of the laser. Finally, an analysis of the experimental spectra of the levels $^4T_1$, $^4T_2$, and ^4E for the same sample has shown that the observed structure cannot be due to Mn^{2+} centers in stacking faults or Mn-Mn pairs whose optical spectra are well known.

The fine and hyperfine structure of the fundamental state can be safety neglected since the cubic field splitting is only $3a=23.6\times10^{-4}$ cm^{-1} (Ref. 24) and since the six hyperfine structure lines extend at most on 0.08 cm^{-1} [hyperfine structure constant $A=-64\times10^{-4}$ cm^{-1} (Ref. 24)].

III. PREVIOUS THEORETICAL MODEL AND COMPARISON WITH EXPERIMENTS

First, we will briefly recall the structure of the $^4T_1$ level at lower energy of Mn^{2+} in tetrahedral symmetry as given by previous experiments and theoretical mode.[8,14] Then, it will be shown that the observed structure for the quasidegenerate states is in disagreement with that previously predicted.

In a CF model, the general Hamiltonian governing the energy levels of d ions in cubic symmetry can be written as

$$H=H_0+H_{\rm cub}+H_{\rm SO}+H_{\rm SS}+H_{\rm el}+H_K+H_{\rm JT}+H_{\rm ext},$$

where H_0 and $H_{\rm cub}$ are the free ion Hamiltonian and the Hamiltonian in a cubic field respectively, $H_{\rm SO}$ and $H_{\rm SS}$ represent the spin-orbit and spin-spin Hamiltonians. $H_{\rm el}$ and H_K are the elastic and kinetic energies associated to the effective vibrational modes. $H_{\rm JT}$ is the Jahn-Teller Hamiltonian describing the electron-nuclear interaction. $H_{\rm ext}$ is a Hamiltonian describing external perturbation effects such as, for example, the uniaxial stress effect, which is essential to determine the symmetry of the effective vibrational modes.

In previous models, the splitting of the quasidegenerate states due to the spin-spin interaction was found to be negligible[14] with respect to previously observed linewidths. Therefore, these models were primarily concerned by the analysis of the spin-orbit interaction. The spin-spin interaction will be considered in Sec. V for the detailed interpretation of the splitting of the quasidegenerate states.

Following Ham's model[1] for the dynamical Jahn-Teller effect on orbital triplets, the influence of the first-order spin-orbit interaction $H_{\rm SO}$ acting on the fundamental vibronic state $|^4T_1,00\rangle$ ($n_\theta=0$, $n_\epsilon=0$), is identical to that of the operator $\exp(-3E_{\rm JT}/2\hbar\omega)H_{\rm SO}$ acting on the electronic state $|^4T_1\rangle$, $E_{\rm JT}$ being the Jahn-Teller energy and $\hbar\omega$ the energy of the effective phonon.

On a real tetragonal basis,[25,26] the diagonal matrix elements of the second-order spin-orbit interaction acting on the fundamental vibronic states are given by

$$\langle {}^4T_{1j},00|H_{\rm SO}^2|{}^4T_{1j},00\rangle=-(f_b/\hbar\omega)\sum_{i=j}\langle {}^4T_{1j}|H_{\rm SO}|{}^4T_{1i}\rangle\langle {}^4T_{1i}|H_{\rm SO}|{}^4T_{1j}\rangle+\sum_{2S+1h_i}\frac{\langle {}^4T_{1j}|H_{\rm SO}|{}^{2S+1}h_i\rangle\langle {}^{2S+1}h_i|H_{\rm SO}|{}^4T_{1j}\rangle}{W({}^4T_1)-W({}^{2S+1}h_i)}.$$

The off-diagonal matrix elements are

$$\langle {}^4T_{1j},00|H_{\rm SO}^2|{}^4T_{1k},00\rangle=-(f_a/\hbar\omega)\langle {}^4T_{1j}|_{\rm SO}|{}^4T_{1i}\rangle\langle {}^4T_{1i}|H_{\rm SO}|{}^4T_{1k}\rangle+e^{-x/2}\sum_{2S+1h_i}\frac{\langle {}^4T_{1j}|H_{\rm SO}|{}^{2S+1}h_i\rangle\langle {}^{2S+1}h_i|H_{\rm SO}|{}^4T_{1k}\rangle}{W({}^4T_1)-W({}^{2S+1}h_i)},$$

where $f_b=e^{-x}G(x)$, with $x=3E_{\rm JT}/\hbar\omega$, $G(x)=\Sigma_{n=1}^{\infty}x^n/n(n!)$, $f_a=e^{-x}G(x/2)$.

The first term appearing in the above expressions is due to the Jahn-Teller coupling between the fundamental and excited vibronic states while the second term describes the Jahn-Teller coupling between the fundamental vibronic state and the excited states of the d^n ion.

As demonstrated in Ref. 8 from an analysis of the uniaxial stress effect, the fluorescent $^4T_1$ level of Mn^{2+} in cubic ZnS is coupled to strains and vibrational modes of E symmetry. Furthermore, the experimental structure of the $^4T_1$ level consisting of only two lines separated by 10 cm^{-1}, the hypothesis of a strong coupling to E vibrational modes was suggested to account for the fine structure of this state. Therefore, the two experimental lines were interpreted as transitions from the fundamental state to the almost degenerate states $|\Gamma_7\rangle$ and $|\Gamma_8'(3/2)\rangle$ for the line at lower energy, and $|\Gamma_6\rangle$ and $|\Gamma_8'(5/2)\rangle$ for the line at higher energy, the splitting being due to the nonreduced matrix elements of the second-order spin-orbit interaction (see Sec. I).

Since it is no longer possible to account for the observed structure of the quasidegenerate states (see Fig. 2) by considering the limit of a strong coupling to E modes, a detailed analysis will now be made of the first-order and second-order spin-orbit interaction in terms of the Huang-Rhys factor, which measures the strength of the coupling to E modes.

The contributions of the first-order and second-order spin-orbit interactions to the splitting of the electronic state $|^4T_1\rangle$ have been calculated by taking a spin-orbit coupling constant of 300 cm^{-1} for the electrons d.[27] The second-order spin-orbit interaction due to the relevant 39 electronic multiplets $^4E(2)$, $^4T_1(3)$, $^4T_2(3)$, $^2E(7)$, $^2T_1(8)$, $^2T_2(10)$, $^6A_1(1)$, $^4A_1(1)$, and $^2A_1(4)$ of the configuration d^5 (the number of multiplets of given spin and symmetry is in parentheses) has been computed by using the following values[8] for the Racah parameters: $B=730$ cm^{-1}, $C=2880$ cm^{-1}, and for the cubic field parameter $Dq=-420$ cm^{-1}. These values for B, C, and Dq approximately account for the energy levels for Mn^{2+} in cubic ZnS. (It can be noted that the spin-orbit splitting of the

TABLE I. Matrix elements of the first-order (first number) and second-order (second number) spin-orbit interaction for the $^4T_1$ level of Mn^{2+} in ZnS. The values chosen for B, C, Dq, and for the spin-orbit coupling constant of the d electrons are given Sec. III. All values are in cm^{-1}.

	$\|\Gamma_6\rangle$	$\|\Gamma_7\rangle$	$\|\Gamma_8(3/2)\rangle$	$\|\Gamma_8(5/2)\rangle$
$\|\Gamma_6\rangle$	−44.25−13.90			
$\|\Gamma_7\rangle$		26.55−39.10		
$\|\Gamma_8(3/2)\rangle$			−17.70−26.04	0+4.01
$\|\Gamma_8(5/2)\rangle$			0+4.01	26.55−27.07

orbital triplet states of Mn^{2+} is not very sensitive to slight variations of these parameters.) The matrix elements of the first- and second-order spin-orbit interactions are given in Table I. Figure 3 represents the computed fundamental vibronic structure in terms of S for two different values for the energy of the effective phonon: $\hbar\omega$=240 and 60 cm^{-1}. The diagonalization was performed by taking into account five phonons. Two very different values for $\hbar\omega$ have been used to show that the vibronic structure is not very sensitive to the energy of the effective phonon. By comparing Fig. 3(b) to that published by Koidl[14] it clearly appears that the vibronic structures obtained by diagonalizing the vibronic Hamiltonian or by using Ham's approximate relations are almost identical. This figure shows that the experimental spectrum could have been accounted for by choosing a value for S between 2.5 and 3.

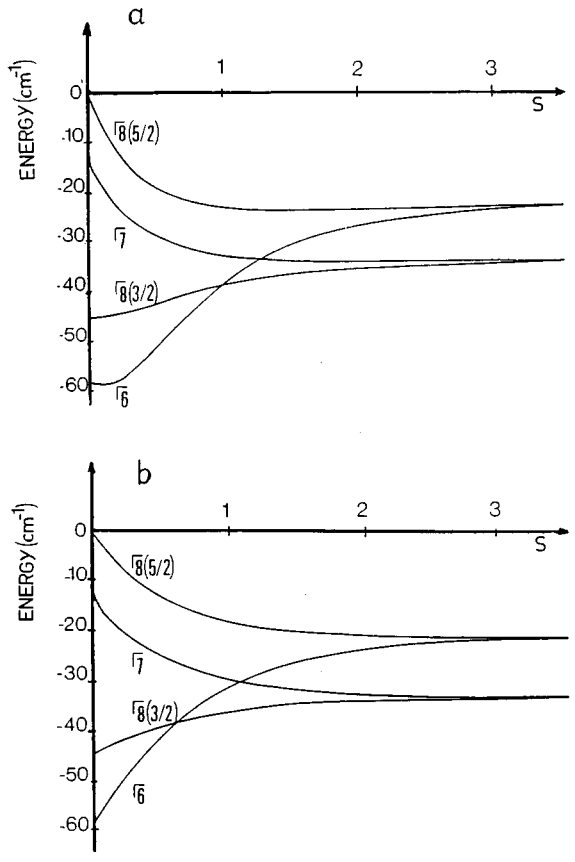

FIG. 3. Theoretical splitting of the $^4T_1(G)$ level of Mn^{2+} in ZnS in terms of the Huang-Rhys factor S. The electronic structure for S=0 is that predicted from the CF model restricted to the d^5 configuration. The energy of the effective phonon is 60 cm^{-1} (a) and 240 cm^{-1} (b). The diagonalization of the vibronic Hamiltonian has been performed by using five phonons.

The dipole strengths will now be considered and it will be shown that the nature of the experimental lines is not that predicted by the above analysis of the energy levels.

In the spinor group Td^*,[26] the relative dipole strengths of the spin and parity forbidden transitions $^6A_1 \rightarrow {}^4T_1$ are given from symmetry considerations by the relation

$$\langle {}^6A_1 J t \tau | H_{SO} | {}^4T_1 J'' t'' \tau'' \rangle \langle {}^4T_1 J'' t'' \tau'' | H_{T2} | {}^4T_1 J' t' \tau' \rangle .$$

H_{SO} is the spin-orbit interaction. In the crystal-field model, H_{T2} is an equivalent operator of symmetry T_2 mimicking the influence of odd parity configurations via the electric dipole moment operator **M** and the odd part of the cubic crystal field of symmetry A_1. In a covalent model such as, for example, a LCAO-MO model, H_{T2} is simply **M** since the matrix elements of **M** are no longer parity forbidden when molecular wave functions are used.

For a $|{}^4T_1\rangle$ state, the RDS's are

$$\sigma({}^6A_1 \rightarrow \Gamma_6) = 45,$$

$$\sigma({}^6A_1 \rightarrow \Gamma_7) = 20,$$

$$\sigma[{}^6A_1 \rightarrow \Gamma_8(3/2)] = 63,$$

$$\sigma[{}^6A_1 \rightarrow \Gamma_8(5/2)] = 22$$

for transitions involving electronic states. For transitions involving vibronic states in the strong JT coupling limit, the RDS of the states $|\Gamma_6\rangle$ and $|\Gamma_7\rangle$ remain unchanged, those of the $|\Gamma_8'\rangle$ states are slightly modified (see the structure of the Γ_8''s in Sec. I):

$$\sigma[{}^6A_1 \rightarrow \Gamma_8'(3/2)] = 62.5,$$

$$\sigma[{}^6A_1 \rightarrow \Gamma_8'(5/2)] = 22.5.$$

The theoretical and experimental RDS's are in correct agreement for all transitions for the indexation of the lines given in Fig. 2.

This indexation of the transitions based on the RDS's is clearly in disagreement with that predicted by the CF model.

In the case of a strong JT coupling to E modes, the CF model predicts that, for increasing energies, the transitions are from the fundamental state to the states $|\Gamma_8'(3/2)\rangle$, $|\Gamma_7\rangle$, $|\Gamma_6\rangle$, and $|\Gamma_8'(5/2)\rangle$ (see Figs. 1 and 3), while, for the indexation given in Fig. 2, the transitions are from the fundamental state to the states $|\Gamma_7\rangle$, $|\Gamma_8'(3/2)\rangle$, $|\Gamma_8'(5/2)\rangle$, and $|\Gamma_6\rangle$.

IV. PHENOMENOLOGICAL MODEL

First, from semiquantitative arguments, it will be shown that the model adopted previously for the structure of the fluorescent level of Mn^{2+} in ZnS has to be entirely reconsidered. Then a phenomenological operator deduced by Ham[1] from symmetry considerations will be used to account for the structure of the studied orbital triplet state.

In the assumption of a strong Jahn-Teller coupling to E modes or in the assumption of a small or negligible first-order spin-orbit interaction with respect to the second-order spin-orbit interaction, the experimental splitting between the gravity centers of the two groups of lines gives a measure of the absolute value of the nonreduced part of the second-order spin-orbit interaction and of the nonreduced part of the spin-spin interaction since these interactions are the only ones that are of importance at the limit of a very strong Jahn-Teller coupling to E modes or when the first-order spin-orbit splitting is small or negligible with respect to the second-order spin-orbit splitting. The sign of this splitting cannot be unambiguously obtained from an analysis of the experimental RDS's since the experimental RDS's of the two lines at lower energy are almost identical to those of the two lines at higher energy. Therefore, the experimental spectrum could be accounted for by associating the lines to transitions to the states $|\Gamma_8'(5/2)\rangle$, $|\Gamma_6\rangle$ and $|\Gamma_7\rangle$, $|\Gamma_8'(3/2)\rangle$ for increasing energy (this indexation will be called ''second indexation'').

From a theoretical point of view, it has been shown in Sec. III that the calculation of the nonreduced part of the second-order spin-orbit interaction accounts very well for the energy separation between the two groups of lines when indexing the experimental lines as shown in Fig. 2. This is the main argument in favor of the calculation of the second-order spin-orbit interaction in a crystal-field model restricted to the d^5 configuration.

By considering now the quasidegenerate states, we observe that there is no simple way to account for the order of these levels. For example, by considering the matrix elements given in Table I and the energy levels given in Fig. 3 in terms of S, it appears that changing the sign of the overall contribution of the second-order spin-orbit interaction and conserving the first-order spin-orbit interaction does not change the order of the quasidegenerate states. Consequently, the correct order for the almost degenerate states cannot be obtained without drastically reducing or even changing the sign of the first-order spin-orbit interaction.

Therefore, the spin-orbit interaction must be reconsidered. As indicated in Sec. I, the structure of the quasidegenerate lines of the fluorescent $^4T_1$ levels of Mn^{2+} in cubic symmetry observed in II-VI compounds and also in GaP has not been resolved.[14] To our knowledge, there is no experimental evidence indicating that the spin-orbit splittings of the electronic states and therefore vibronic states deduced from the CF model are correct.

When considering that the calculations of the spin-orbit interaction performed until now are of no help in interpreting the experimental spectrum, we can only say from an analysis of the RDS's that the two less intense lines are to be associated to the states $|\Gamma_7\rangle$ or $|\Gamma_8'(5/2)\rangle$, the most intense lines being associated to the states $|\Gamma_6\rangle$ or $|\Gamma_8'(3/2)\rangle$. (The two groups of lines shown in Fig. 2 having almost the same amplitude, it is not possible to unambiguously associate the lines to the transitions given in this figure.) Among the four possible indexations of the lines, those associating two almost degenerate lines to two $|\Gamma_8\rangle$ states are to be rejected since they are not compatible with the uniaxial stress effect analyzed in Ref. 8. Therefore, only two indexations are allowed: the first indexation given in Fig. 2 and the second indexation defined above.

A phenomenological model, deduced from symmetry considerations due to Ham,[1] will now be presented, which gives the energy levels and RDS's in terms of three parameters. Following Ham's method,[1] the first- and second-order spin-orbit interactions and the spin-spin interaction are given by the equivalent operator acting on the electronic states:

$$H_{\rm eq}=\alpha \mathbf{l}\cdot\mathbf{S}+\beta(\mathbf{l}\cdot\mathbf{S})^2+\gamma\sum_i (l_i^2S_i^2),$$

where α, β, and γ are three constants or parameters depending on the spin-orbit and spin-spin interactions described by $H_{\rm eq}$. $i=x,y,z$. (We use the notation α,β,γ instead of Koidl's notation[14] χ,μ,ρ, which will describe, in the next section, the *electronic* spin-orbit interaction.) $\boldsymbol{l}$ is an effective orbital momentum, for a $^4T_1$ state, $l=1$ and $S=3/2$. When considering vibronic interactions, it is convenient to introduce operators spanning the irreducible representations of Td, such that[1]

$$(\boldsymbol{l}\cdot\boldsymbol{S})^2=-(1/2)\boldsymbol{l}\cdot\boldsymbol{S}+(2/3)(l_\theta S_\theta+l_\epsilon S_\epsilon)+(1/2)(l_\xi S_\xi+l_\eta S_\eta+l_\zeta S_\zeta)+(1/3)\boldsymbol{l}^2\boldsymbol{S}^2,$$

$$\times\sum_i (l_i^2S_i^2)=(2/3)(l_\theta S_\theta+l_\epsilon S_\epsilon)+(1/3)\boldsymbol{l}^2\boldsymbol{S}^2.$$

$H_{\rm eq}$ can now be written as

$$H_{\rm eq}=c_{T1}\boldsymbol{l}\cdot\boldsymbol{S}+c_E(2/3)(l_\theta S_\theta+l_\epsilon S_\epsilon)+c_{A1}(1/3)\boldsymbol{l}^2\boldsymbol{S}^2+c_{T2}(1/2)(l_\xi S_\xi+l_\eta S_\eta+l_\zeta S_\zeta).$$

The index Γ in the constants or parameters $c_\Gamma s$ indicate that the operators span the representation Γ of Td. The $c_\Gamma s$, which are simply related to α, β, and γ by $c_{T1}=\alpha-\beta/2$, $c_E=\beta+\gamma$, and $c_{T2}=\beta$, will be expressed in terms of the constants or parameters describing the spin-orbit and spin-spin interaction in the next section. The term in c_{A1} describes the shift common to the fine-structure lines. c_{T1}, c_E, and c_{T2} will now be considered as fitting parameters describing the splittings of the fine-structure lines.

These parameters can be deduced from the energy separation between the gravity centers of the groups of lines: $\Delta=\pm 9.48\ \mathrm{cm}^{-1}$ (the minus and plus signs correspond to the first and second indexations, respectively) and the splittings of the quasidegenerate states $W\Gamma_6-W\Gamma_8'(5/2)=0.60\ \mathrm{cm}^{-1}$ and $W\Gamma_8'(3/2)-W\Gamma_7=0.70\ \mathrm{cm}^{-1}$ for $\Delta<0$, and $W\Gamma_6-W\Gamma_8'(5/2)=0.70\ \mathrm{cm}^{-1}$ and $W\Gamma_8'(3/2)-W\Gamma_7=0.60\ \mathrm{cm}^{-1}$ for $\Delta>0$.

In Td^*, the matrix elements of H_{eq} are

$$\langle\Gamma_6|H_{\mathrm{eq}}|\Gamma_6\rangle=(5/2)c_{A1}+c_E-(5/2)c_{T1}+(3/2)c_{T2},$$

$$\langle\Gamma_7|H_{\mathrm{eq}}|\Gamma_7\rangle=(5/2)c_{A1}-c_E+(3/2)c_{T1}+(3/2)c_{T2},$$

$$\langle\Gamma_8(3/2)|H_{\mathrm{eq}}|\Gamma_8(3/2)\rangle=(5/2)c_{A1}-(4/5)c_E-c_{T1}-(6/5)c_{T2},$$

$$\langle\Gamma_8(5/2)|H_{\mathrm{eq}}|\Gamma_8(5/2)\rangle=(5/2)c_{A1}+(4/5)c_E+(3/2)c_{T1}-(3/10)c_{T2},$$

$$\langle\Gamma_8(3/2)|H_{\mathrm{eq}}|\Gamma_8(5/2)\rangle=(3/5)(c_E-c_{T2}).$$

The coefficients c_{T1}, c_E, and c_{T2} can be obtained by diagonalyzing the matrix for the Γ_8's and by using a Taylor series approximation to first order since, as deduced from the experimental spectrum, the terms in c_{T1} and c_{T2} are more than an order of magnitude smaller than the terms in c_E. From this method the energies of the Γ_8's are given by

$$\langle\Gamma_8'(3/2)|H_{\mathrm{eq}}|\Gamma_8'(3/2)\rangle=(5/2)c_{A1}+c_E+(5/4)c_{T1}-(3/4)c_{T2},$$

$$\langle\Gamma_8'(5/2)|H_{\mathrm{eq}}|\Gamma_8'(5/2)\rangle=(5/2)c_{A1}-c_E-(3/4)c_{T1}-(3/4)c_{T2}.$$

The c_Γ are given by

$$c_{T1}=\tfrac{1}{6}[-W\Gamma_6+W\Gamma_8'(5/2)-W\Gamma_8'(3/2)+W\Gamma_7],$$

$$c_E=\tfrac{1}{6}[2W\Gamma_8'(5/2)+W\Gamma_6-2W\Gamma_8'(3/2)-W\Gamma_7],$$

$$c_{T2}=\tfrac{1}{18}\{3[W\Gamma_6-W\Gamma_8'(5/2)]+5[W\Gamma_7-W\Gamma_8'(3/2)]\}.$$

For $\Delta=-9.48\ \mathrm{cm}^{-1}$, we obtain $c_{T1}=-0.216\ \mathrm{cm}^{-1}$, $c_E=4.740\ \mathrm{cm}^{-1}$, and $c_{T2}=-0.094\ \mathrm{cm}^{-1}$, the RDS's being $\sigma(^6A_1\rightarrow\Gamma_6)=45$, $\sigma(^6A_1\rightarrow\Gamma_7)=20$, $\sigma[^6A_1\rightarrow\Gamma_8'(3/2)]=62.1$, and $\sigma[^6A_1\rightarrow\Gamma_8'(5/2)]=22.9$.

For $\Delta=+9.48\ \mathrm{cm}^{-1}$, we get $c_{T1}=-0.213\ \mathrm{cm}^{-1}$, $c_E=-4.952\ \mathrm{cm}^{-1}$, and $c_{T2}=-0.049\ \mathrm{cm}^{-1}$. The RDS's are $\sigma(^6A_1\rightarrow\Gamma_6)=45$, $\sigma(^6A_1\rightarrow\Gamma_7)=20$, $\sigma[^6A_1\rightarrow\Gamma_8'(3/2)]=62.8$, and $\sigma[^6A_1\rightarrow\Gamma_8'(5/2)]=22.2$.

V. PHYSICAL MODEL AND DISCUSSION

By taking into account explicitly the spin-orbit and spin-spin interactions, and vibronic coupling to E modes, the c_Γ are given by

$$c_{T1}=(\chi-\mu/2)e^{-3S/2}-K_1/2,$$

$$c_E=\mu+\rho+K_1+K_2+c_2+c_3,$$

$$c_{T2}=(\mu+c_2)e^{-3S/2}+K_1.$$

where $\chi=\chi_1+\chi_2$. The term in χ_1 describes the electronic first-order spin-orbit interaction. The terms in χ_2, μ, and ρ are related to the reduced and nonreduced part of the electronic second-order spin-orbit interaction involving the excited electronic states. The terms in K_1 and K_2 are related to the terms in f_a and f_b defined in Sec. III by $K_1=-\chi_1^2 f_a/\hbar\omega$, and $K_1+K_2=-\chi_1^2 f_b/\hbar\omega$. The coefficients $c_2=2c_1$ and c_3, which describe the spin-spin interaction, have been calculated in the CF model restricted to the d^5 configuration by Koidl,[14] for the fluorescent level and the $^4T_2$ level at lower energy of Mn^{2+} in ZnS and ZnSe. For the fluorescent level of Mn^{2+} in ZnS, $c_2=-0.292\ \mathrm{cm}^{-1}$ and $c_3=-0.037\ \mathrm{cm}^{-1}$.[14]

The parameters for the physical model are E_{JT} and $\hbar\omega$ or S and $\hbar\omega$ for the vibronic interactions. χ, μ, and ρ are considered fitting parameters for the spin-orbit interaction. The theoretical values for the coefficients c_2 and c_3, which describe the spin-spin interaction, are the only theoretical values used in the following calculations.

From the above relations, we get

$$\chi=(c_{T1}+c_{T2}/2)e^{3S/2}-c_2/2$$

and

$$\mu+\rho=c_E-K_1-K_2-c_2-c_3,$$

$$\mu=(c_{T2}-K_1)e^{3S/2}-c_2.$$

χ, $\mu+\rho$, and μ have been calculated in terms of S, for $\hbar\omega=240$ and $60\ \mathrm{cm}^{-1}$. The results are given in Table II and Fig. 4 for the first and the second indexation. This means that, for a given value for S and $\hbar\omega$, the values obtained for χ, $\mu+\rho$, and μ permit an exact fitting of the experimental spectrum.

For the first indexation given in Fig. 2 ($\Delta<0$), the fitting of the experimental spectrum is obtained for decreasing values of χ from -0.11 to $-104\ \mathrm{cm}^{-1}$ when S increases from 0 to 4 (see Fig. 4). These values for χ are to be compared to $+13.5\ \mathrm{cm}^{-1}$ as given by the CF model ($\chi_1=17.7\ \mathrm{cm}^{-1}$ and $\chi_2=-4.2\ \mathrm{cm}^{-1}$).

It must be noted that χ is negative whatever the value for S, and that for S greater than 2.5, χ becomes very large and negative.

Therefore, a correct fitting of the experimental spectrum can only be obtained by taking a value for χ whose sign is opposite to that predicted by the model restricted to the d^5 configuration.

For the first indexation, when $\hbar\omega=60\ \mathrm{cm}^{-1}$, $\mu+\rho$ increases slightly from 5.07 to $6.21\ \mathrm{cm}^{-1}$ when S increases from 0 to 3, then $\mu+\rho$ increases rapidly to $21.87\ \mathrm{cm}^{-1}$ for $S=4$. For $\hbar\omega=240\ \mathrm{cm}^{-1}$, the values for $\mu+\rho$ are almost

TABLE II. Values of the fitting parameters for the spin-orbit interaction in terms of S. χ, μ, and ρ are defined in Sec. V. $\hbar\omega$ is the energy of the effective phonons. All values are in cm^{-1}.

S		0	1	2	3	4
χ	($\Delta<0$)	−0.11	−1.02	−5.08	−23.26	−104.75
χ	($\Delta>0$)	−0.09	−0.92	−4.63	−21.26	−95.78
$\mu+\rho$	($\Delta<0$, $\hbar\omega=60$)	5.07	5.07	5.15	6.21	21.87
$\mu+\rho$	($\Delta<0$, $\hbar\omega=240$)	5.07	5.07	5.09	5.35	9.27
$\mu+\rho$	($\Delta>0$, $\hbar\omega=60$)	−4.62	−4.62	−4.55	−3.67	9.43
$\mu+\rho$	($\Delta>0$, $\hbar\omega=240$)	−4.62	−4.62	−4.60	−4.38	−1.11
μ	($\Delta<0$, $\hbar\omega=60$)	0.20	−0.12	−1.41	−5.52	0.54
μ	($\Delta<0$, $\hbar\omega=240$)	0.20	−0.12	−1.54	−7.46	−27.88
μ	($\Delta>0$, $\hbar\omega=60$)	0.24	0.08	−0.54	−1.95	12.26
μ	($\Delta>0$, $\hbar\omega=240$)	0.24	0.07	−0.65	−3.57	−11.51

identical to those obtained with the low-energy phonon for $S<3$, then $\mu+\rho$ increases to 9.27 cm^{-1} for $S=4$. As already shown in Sec. III, the value for $\mu+\rho$, which is related to Δ by $\mu+\rho=-\Delta/2-K_1-K_2-c_2-c_3$, is correctly given by the CF model restricted to the d^5 configuration, but for $S<3$ only. It can be noted that $\Delta\sim-2(\mu+\rho)$ when $S<3$, since the term $-K_1-K_2-c_2-c_3$ equals $+1.48$ cm^{-1} at most for $S=3$. For $S>3$, this approximation is no longer valid since $-K_1-K_2$ increases rapidly to 16.80 cm^{-1} for $S=4$.

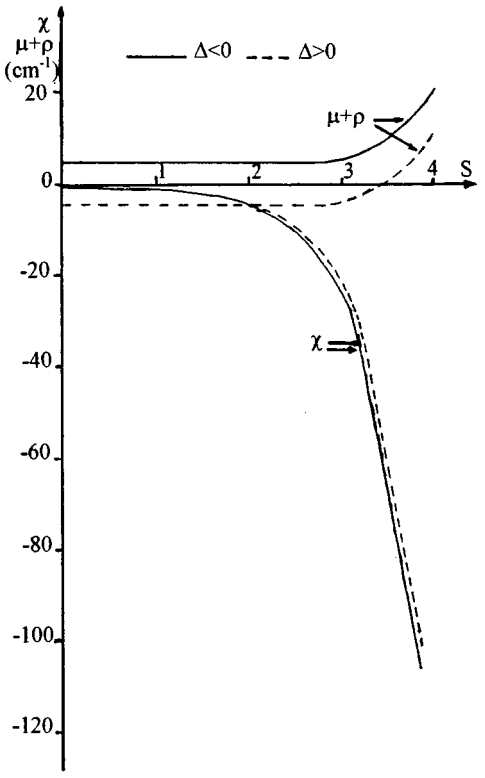

FIG. 4. Values of the parameters χ and $\mu+\rho$ describing the spin-orbit interaction in terms of the Huang-Rhys factor S. The energy of the effective phonon is $\hbar\omega=60$ cm^{-1}. The solid lines correspond to the first indexation of the fine structure lines of the $^4T_1$ level as shown in Fig. 2. The broken lines correspond to the second indexation defined in Sec. IV.

Since the first-order spin-orbit interaction predicted by the model restricted to the d^5 configuration is not valid, it is no longer possible to assume that the second-order spin-orbit interaction given by the CF model is correct. This means that the ''second indexation'' cannot be rejected, this indexation being obtained by changing the sign of the second-order spin-orbit interaction given by the CF model. In that case, Δ is positive. For $\hbar\omega=240$ or 60 cm^{-1}, the fitting of the energy levels is obtained for values χ in terms of S, which are almost identical to those obtained for the first indexation.

Therefore, for both indexations, χ is negative.

Concerning the spin-spin interaction, Table II shows that its contribution to χ becomes negligible for $S>1$ (for $S>1$, $\chi<-1.02$ cm^{-1} for $\Delta<0$, and $\chi<-0.92$ cm^{-1} for $\Delta>0$, these values are to be compared to $c_2/2=-0.15$ cm^{-1}). Its contribution to μ becomes negligible for $S>3$ and its contribution to $\mu+\rho$ is negligible whatever S.

VI. LIGAND-FIELD MODEL FOR THE FIRST-ORDER SPIN-ORBIT INTERACTION

Recently, a systematic study of the influence of covalency on Mn^{2+} in II-VI compounds was performed. First, a covalent model has been developed to interpret the OLCC to E strains of the orbital triplet states of Mn^{2+} in II-VI compounds.[20] In this study, molecular wave functions were obtained for the orbital triplet states of Mn^{2+} in ZnS and ZnSe, which allowed one to account for the experimental OLCC's. Then, a covalent model for the SLCC's of Mn^{2+} in II-VI compounds has been developed.[21] By using the molecular wave functions, which accounted very well for the OLCC's and the molecular spin-orbit interaction defined by Misetich and Buch,[19] a model was elaborated that correctly accounted for the SLCC's of Mn^{2+} in ZnS, ZnSe, ZnTe, and CdTe. It was shown that the SLCC's whose moduli differ by almost two orders of magnitude primarily depend on the spin-orbit interaction of the electrons p of the ligands.

In the forthcoming analysis of the spin-orbit interaction in the triplet states of Mn^{2+} in II-VI compounds, we will use the molecular wave functions described in detail in Ref. 20.

In a covalent model the relevant operator describing the spin-orbit interaction is the molecular spin-orbit interaction H_{SOm}, which acts on the electrons of the metal and of the

ligands, and depends on the interatomic distances and angles. As shown by Misetich and Buch,[19] H_{SOm} can be written as

$$H_{\mathrm{SOm}}=\sum_i \zeta_M(r_{iM})\boldsymbol{l}_{iM}\cdot\mathbf{s}_i+\sum_i\sum_L \zeta_L(r_{iL})\boldsymbol{l}_{iL}\cdot\mathbf{s}_i,$$

where $\boldsymbol{l}_{iM}$ and $\boldsymbol{l}_{iL}$ are one-electron orbital operators for the metal and the ligands, respectively. ζ_M and ζ_L are the spin-orbit coupling constants, defined by Blume and Watson,[27] of the electrons $3d$ of the metal and of the electrons np ($n=3$ for S and $n=4$ for Se) of ligands, respectively.

It is convenient to write H_{SOm} in terms of the molecular angular momentum τ_u^i of electron i and the complex components of the spin operators[26] as

$$H_{\mathrm{SOm}}=\sum_{qi}\tau_u^i\mathbf{s}_q^i.$$

In this expression, $u=x$ or y if $q=\pm1$ and $u=z$ if $q=0$. The operators τ_u^i are

$$\tau_u^i=\zeta_M(r_{iM})\boldsymbol{l}_{Mu}^i+\zeta_L(r_{iL})\Omega_u^i,$$

Ω^i being the angular momentum of electron i of the ligands.

The relevant monoelectronic molecular orbitals $4t_2$ and $2e$ (of the half-filled shells), which are linear combinations of atomic orbitals $3d$ and $4p$ of Mn, and the valence orbitals $3s$ and $3p$ of sulfur, are described in detail in Ref. 20. They are written in terms of the monoelectronic orbitals of the electrons $3d$ and $4p$ of metal, and in terms of the orbitals σs, σp, and πp of ligands as

$$|t_2\gamma\rangle=a^d|dt_2\gamma\rangle+a^p|pt_2\gamma\rangle+a^{\sigma s}|\sigma st_2\gamma\rangle+a^{\sigma P}|\sigma pt_2\gamma\rangle+a^{\pi P}|\pi pt_2\gamma\rangle,$$

where $\gamma=\xi$, η, or ζ refers to the components of the molecular monoelectronic level $4t_2$ and

$$|e\gamma'\rangle=b^d|de\gamma'\rangle+b^{\pi p}|\pi pe\gamma'\rangle,$$

where $\gamma'=\theta$ or ϵ refers to the components of the molecular monoelectronic level $2e$.

The a's for the orbitals $4t_2$ and b's for the orbitals $2e$ result from the diagonalization of the molecular Hamiltonian. The levels $1t_2$, $2t_2$, $3t_2$, and $1e$ are filled, the levels $4t_2$ and $2e$ are half filled.

Then, the multielectronic wave functions for the orbital triplet states are obtained by diagonalizing the matrix of Sugano, Tanabe, and Kamimura[28] for the three $|^4T_1\rangle$ states at lower energy. Explicitly we get

$$|^4T_{1u}^q\rangle=a_1^q|^4T_{1u}^q(4t_2^42e)\rangle+a_2^q|^4T_{1u}^q(4t_2^32e^2)\rangle+a_3^q|^4T_{1u}^q(4t_2^22e^3)\rangle,$$

where $q=1,2,3$ refers to the three levels $^4T_1$: $u=x$, y, or z.

The matrix elements of the molecular spin-orbit interaction can now be expressed in terms of the matrix elements of the operator τ. The relevant matrix elements of τ for the monoelectronic wave functions $2e$ and $4t_2$ are

$$\zeta et_2=\frac{i}{2}\langle e\epsilon|\tau_z|t_2\zeta\rangle$$

and

$$\zeta t_2t_2=\frac{i}{2}\langle t_2\xi|\tau_z|t_2\eta\rangle.$$

Explicitly ζet_2 and ζt_2t_2 are given in terms of the mixing coefficients of the monoelectronic wave functions and of the spin-orbit constants of the metal and of the ligands by

$$\zeta et_2=a^db^d\zeta_M+\frac{1}{(2\sqrt{3})}b^{\pi p}(a^{\pi p}+a^{\sigma p}\sqrt{2})\zeta_L$$

and

$$\zeta t_2t_2=(a^da^d-a^pa^p)\zeta_M+a^{\pi p}(a^{\sigma p}\sqrt{2}-a^{\pi p}/2)\zeta_L.$$

We can note here that in the CF model restricted to the configuration d^5, $\zeta t_2t_2=\zeta et_2=\zeta_M$, since in this case, $a^d=b^d=1$, the other coefficients being zero.

By using the mixing parameters for the triplet states obtained from the values of B, C, and Dq given in Sec. III, we get for the studied $|^4T_1\rangle$ state:

$$\chi_1=0.1438\zeta t_2t_2-0.0848\zeta et_2.$$

In the self-consistent model, the molecular orbitals and the physical constants depend on few constants or parameters. The molecular orbitals that intervene in ζt_2t_2 and ζet_2 were computed in Ref. 20.

Slight variations of the interatomic distance, of the effective charge Q_{Lat} of the lattice and Q_M of the metal, and of a constant C_{mad} describing the crystal electric field were considered in Ref. 20. C_{mad} was defined in the following manner: diagonal and off-diagonal matrix elements of the crystal electric field due to the nearest neighbors of the metal atom and of the nearest neighbors of the ligands have been calculated directly; C_{mad} represents the contribution to the Madelung energy of the remaining atoms of the crystal. By including the electric field of the crystal in this manner, molecular wave functions were obtained that correctly fitted the OLCC's of the orbital triplet states $|^4T_1\rangle$ and $|^4T_2\rangle$ of Mn in ZnS and ZnSe, and the SLCC's of Mn in II-VI compounds.[20,21]

The spin-orbit coupling constants of the electrons $3d$ of Mn and $3p$ of S were obtained by interpolating the spin-orbit coupling constants given by Blume and Watson[27] for various ionization states of the atoms. Explicitly (all values are in cm^{-1}):

$$\zeta_M(\mathrm{Mn})=286+47(Q_M-1),$$

$$\zeta_L(\mathrm{S})=298+65(Q_L+1).$$

The molecular orbitals were those obtained from one set of constants or parameters that accounted for the OLCC's and SLCC's of Mn. The interatomic distance Mn-S of 4.56 a.u. was chosen to be slightly greater than the interatomic distance Zn-S of 4.41 a.u. to account for a slightly greater covalent radius of Mn than of Zn, $Q_{\rm lat}=\pm 0.80$, $Q_M=0.97$, and $C_{\rm mad}=1.40$.

Straightforward calculations gave $\zeta t_2 t_2=130.8\ \mathrm{cm}^{-1}$, $\zeta e t_2=205\ \mathrm{cm}^{-1}$, and $\chi_1=+1.42\ \mathrm{cm}^{-1}$. This strong reduction of χ_1 with respect to the value of $+17.7\ \mathrm{cm}^{-1}$ as deduced from the model restricted to the d^5 configuration is due to the fact that for the studied $^4T_1$ level of Mn in ZnS, χ_1 depends on two terms having approximately the same magnitude and opposite signs.

In order to have an idea of the trend of the first-order spin-orbit interaction of the fluorescent state of Mn in II-VI compounds, a computation of χ_1 was also performed for ZnSe. The mixing parameters for the $^4T_1$ levels were obtained by using the following values for the Racah parameters: $B=740\ \mathrm{cm}^{-1}$, $C=2740\ \mathrm{cm}^{-1}$, and $Dq=-405\ \mathrm{cm}^{-1}$.[15] From these values for B, C, and Dq, we got

$$\chi_1=0.1448\zeta t_2 t_2-0.0880\zeta e t_2 .$$

By comparing this expression to that obtained for Mn in ZnS, it can be noted that χ_1 is not very sensitive to the values of B, C, and Dq.

By using the spin-orbit coupling constant of the electrons $4p$ of Se given by[27]

$$\zeta_L(\mathrm{Se})=1353+297(Q_L+1),$$

and the molecular orbitals computed in Ref. 20 by taking interatomic distances Mn-Se of 4.76 a.u. and Zn-Se of 4.61 a.u., $Q_{\rm lat}=\pm 0.7$, $Q_M=0.74$, and $C_{\rm mad}=1.25$, we obtained $\zeta t_2 t_2=-321\ \mathrm{cm}^{-1}$, $\zeta e t_2=+125\ \mathrm{cm}^{-1}$, and $\chi_1=-57.5\ \mathrm{cm}^{-1}$.

It is important to note that this value for χ_1 is of opposite sign and that its modulus is more than three times greater than the value given by the CF model restricted to the d^5 configuration (by taking $\zeta_{3d}=300\ \mathrm{cm}^{-1}$ and the values for B, C, and Dq given above, the CF model gives $\chi_1=+17.1\ \mathrm{cm}^{-1}$ for Mn^{2+} in ZnSe).

By comparing now the theoretical values for χ_1 obtained for ZnS and ZnSe, we note that $\zeta e t_2$ is positive in both cases while the sign of $\zeta t_2 t_2$ changes when passing from ZnS to ZnSe. The values for $\zeta t_2 t_2$ and $\zeta e t_2$ are very different for Mn in ZnS and ZnSe, primarily because ζ_L(Se) is four to five times greater than ζ_L(S) and, to a lesser extent, because of slight variations of the mixing coefficients of the monoelectronic wave functions.

As in the case of the SLCC's to E strains, this study shows that the spin-orbit dependent physical constants of Mn in II-VI compounds very strongly depend on the spin-orbit coupling constants of the electrons p of the ligands.

For Mn in ZnS, by slightly modifying the parameters intervening in the LF model, in particular the electric crystal field, it probably would be possible to get molecular wave functions, which could give slightly negative values for χ_1 as well as correct values for the OLCC's and SLCC's.

Since the LF model predicts a small value for χ_1, then a small to moderate JT coupling to E modes of the $^4T_1(G)$ level of Mn in ZnS is expected from this model. Table II and Fig. 4, which give the values for χ in terms of S permitting an exact fit of the experimental structure, show that small negative values for χ are obtained for $S\leqslant 2$, corresponding to $\chi\geqslant -5\ \mathrm{cm}^{-1}$.

Of course, the structure of the $^4T_1(G)$ level depends on the second-order spin-orbit interaction, which could be computed from the proposed LF model. However, the diagonal and off-diagonal parts of the second-order spin-orbit interaction are much more difficult to handle in the LF model than the first-order spin-orbit interaction.

VII. CONCLUSION

The four fundamental vibronic lines of the fluorescent orbital triplet state $|^4T_1\rangle$ of Mn^{2+} coupled to E vibrational modes have been observed in pure cubic ZnS and the electronic and vibronic models for the $^4T_1$ state have been reconsidered.

From a very detailed analysis of the experimental and theoretical splittings and dipole strengths of the quasidegenerate states, it has been shown, first, that the order of these states is in contradiction with that predicted by previous electronic and vibronic models.

Then, a model has been elaborated in which the first- and second-order spin-orbit interaction, and the spin-spin interaction are described by three fitting parameters, which can be deduced from the splittings of the quasidegenerate states and from the energy separation between the centers of gravity of the quasidegenerate states. From an analysis of the RDS's, two indexations of the experimental lines have been proposed, which perfectly account for the energy levels and correctly account for the RDS's.

Relations between the parameters describing the spin-orbit interaction and the Huang-Rhys factor were defined, which exactly accounted for the energy levels of the $^4T_1$ level. An analysis of the electronic and vibronic interactions contributing to the fitting parameters has shown that the structure of the studied state can be accounted for if the splitting of the electronic state due to the spin-orbit interaction in $\boldsymbol{l}\cdot\boldsymbol{S}$ is inversed with respect to that previously predicted for d electrons.

To account for this very unexpected result, a calculation of the first-order spin-orbit interaction has been performed in the self-consistent LCAO-MO model previously developed to analyze physical constants depending on the molecular spin-orbit interaction of d^5 ions in II-VI compounds. It has been shown that the molecular model can account for a very strong reduction of the first-order spin-orbit interaction and even for a change of sign of this interaction with respect to that given by the CF model and that the first-order spin-orbit interaction for the fluorescent state of Mn^{2+} critically depends on the nature of the ligands as was shown by comparing this interaction for Mn in ZnS and ZnSe.

Concerning the strength of the coupling to E modes, a comparison of values of χ, in terms of S, which exactly fit the vibronic structure with plausible values for χ obtained

from the LF model indicate that a weak to intermediate JT coupling corresponding to $S \leqslant 2$ can account for the observed structure of the $^4T_1$ level of Mn in ZnS.

Concerning the proposed indexations of the lines, it is suggested that a high-resolution study of the Zeeman effect, implying a detailed comparison for both indexations of the experimental and theoretical energies and RDS's in terms of the magnetic field, could unambiguously give the correct indexation. Due to the lack of a detailed study of the RDS for both indexations, the studies of the Zeeman effect performed until now on the fluorescent levels of Mn^{2+} in ZnS (Ref. 17) and GaP (Ref. 18) do not permit one to select the indexation.

ACKNOWLEDGMENTS

Thanks are due to C. Naud for very helpful discussions on the vibronic structure of orbital triplet states and to J. Mahrt for his help during the development of the experimental setup.

[1] F. S. Ham, Phys. Rev. **138**, A1727 (1965).

[2] F. S. Ham, W. M. Schwarz, and M. C. M. O'Brien, Phys. Rev. **185**, 548 (1969); F. S. Ham and G. A. Slack, Phys. Rev. B **4**, 777 (1971).

[3] A. Abragam and B. Bleaney, *Electron Paramagnetic Resonance of Transition Ions* (Clarendon, Oxford, 1969); F. S. Ham, in *Electron Paramagnetic Resonance*, edited by S. Geschwind (Plenum, New York, 1972).

[4] R. Engelman, *The Jahn-Teller Effect in Molecules and Crystals* (Wiley, New York, 1972).

[5] Very detailed molecular orbital theories concerning the optical levels of d^5 ions and particularly Mn^{2+} ions have been developed, for example, by C. J. Ballhausen and H. B. Gray, *Molecular Orbital Theory* (Benjamin, New York, 1965). See also A. D. Liehr and C. J. Ballhausen, Phys. Rev. **106**, 1161 (1957); L. L. Lohr, Jr., J. Chem. Phys. **45**, 3611 (1966). More recently, simplified semi-empirical models have been used by A. J. O'Neill and W. Allen, Solid State Commun. **46**, 833, (1983); S. W. Berniacki, Phys. Status Solidi B **118**, 525 (1983); **131**, 349 (1985); **132**, 557 (1985); A. Zunger, in *Solid State Physics*, edited by H. Ehrenreich and D. Turnbull (Academic, New York, 1986), Vol. 39, p. 275.

[6] The influence of covalency on the magnetic properties of d^n ions has been reviewed, for example, by J. Owen and J. H. M. Thornley, Rep. Prog. Phys. **29**, 675 (1966). See also Ref. 3.

[7] D. Langer and S. Ibuki, Phys. Rev. **138**, A809 (1965).

[8] R. Parrot, C. Naud, C. Porte, D. Fournier, A. C. Boccara, and J. C. Rivoal, Phys. Rev. B **17**, 1057 (1978).

[9] D. Langer and H. J. Richter, Phys. Rev. **146**, 554 (1966).

[10] A. T. Vink and G. G. P. Van Gorkom, J. Lumin. **5**, 379 (1972).

[11] M. T. Vala, C. J. Ballhausen, R. Dingle, and S. L. Holt, Mol. Phys. **23**, 217 (1972).

[12] M. Y. Chen, D. S. McClure, and E. I. Solomon, Phys. Rev. B **6**, 1690 (1972).

[13] R. Romestain, thesis, University of Paris, 1972.

[14] P. Koidl, Phys. Status Solidi **74**, 477 (1976).

[15] R. Parrot, C. Naud, and F. Gendron, Phys. Rev. B **13**, 3748 (1976).

[16] C. Naud, C. Porte, F. Gendron, and R. Parrot, Phys. Rev. B **20**, 3333 (1979).

[17] D. Fournier, A. C. Boccara, and J. C. Rivoal, J. Phys. C **10**, 113 (1977).

[18] G. Hofman, F. G. Anderson, and J. Weber, Phys. Rev. B **43**, 9711 (1991).

[19] A. A. Misetich and T. Buch, J. Chem. Phys. **42**, 2524 (1964).

[20] D. Boulanger and R. Parrot, J. Chem. Phys. **87**, 1469 (1987).

[21] R. Parrot and D. Boulanger, Phys. Rev. B **47**, 1849 (1993).

[22] R. Parrot, A. Geoffroy, C. Naud, W. Busse, and H. E. Gumlich, Phys. Rev. B **23**, 5288 (1981).

[23] U. W. Pohl and H. E. Gumlich, Phys. Rev. B **40**, 1194 (1989).

[24] J. Schneider, S. R. Sircar, and A. Räuber, Z. Naturforsch. **18a**, 980 (1963).

[25] J. S. Griffith, *The Theory of Transition Metal Ions* (Cambridge University Press, 1971).

[26] J. S. Griffith, *The Irreducible Tensor Method for Molecular Symmetry Groups* (Prentice-Hall, Englewood Cliffs, NJ, 1962).

[27] M. Blume and R. E. Watson, Proc. R. Soc. London Ser. A **271**, 565 (1963).

[28] Sugano, Y. Tanabe, and H. Kamimura, *Multiplets of Transition Metal Ions in Crystals* (Academic, New York, 1970).